arXiv:hep-lat/9408001v1 1 Aug 1994

KYUSHU-HET-17, SAGA-HE-65

Chiral perturbation theory, finite size effects and the three-dimensional XY model

Shin-ichi Tominaga* and Hiroshi Yoneyama†**

Department of Physics
Kyushu University
Fukuoka, 812 JAPAN

† Department of Physics
Saga University
Saga, 840 JAPAN

Abstracts

We study finite size effects of the d=3 XY model in terms of the chiral perturbation theory. We calculate by Monte Carlo simulations physical quantities which are, to order of $(1/L)^2$, uniquely determined only by two low energy constants. They are the magnetization and the helicity modulus (or the Goldstone boson decay constant) in infinite volume. We also pay a special attention to the region of the validity of the two possible expansions in the theory.

---

* e-mail:tomi1scp@mbox.nc.kyushu-u.ac.jp

** e-mail:yoneyama@math.ms.saga-u.ac.jp

1. Introduction

One has to cope with finite size effects in study of numerical simulations on lattices. Recently Hasenfratz and Leutwyler [1] have applied to this issue the chiral perturbation theory [2] which is systematic and quite alternative to the finite size scaling [3] [4]. The chiral perturbation theory is originally a low energy effective theory of QCD and it has some systematic expansions in momentum of pions. For a system in a finite box with volume $V = L^d$, which involves Goldstone boson(s), long range properties are dominated by the finite mass of Goldstone bosons. By controlling its effect in a way, the chiral perturbation theory enables one to calculate physical quantities in a systematic series in terms of $1/L$. As a way of controlling, an external source coupled to the field in consideration plays an important role. There are two manners, one is called the ϵ-expansion, and another is the p-expansion, which result in the series in different powers of $1/L$. Each of them has its own characteristic region in the space of the the external source j. The ϵ-expansion characterizes the domain where $j \sim L^{-d}$, while the p-expansion corresponds to $j \sim L^{-2}$.

In the present paper we consider the $d = 3$ dimensional O(2) non-linear sigma model, or XY-model. Though this model is simple, it is a good laboratory for studying the critical phenomena of the lattice scalar field theory with a global symmetry. From a realistic point of view as well, it is significant in connection with superfluid ^{4}He [5]. This model has widely been studied [6] [7] [8] [9] [10] [11] [12] [13]. It is therefore suitable to choose this model and to compare with those analysis in order to check whether the chiral perturbation theory works. The advantage of taking the model of the dimension three ($d = 3$) in the chiral perturbation theory is that finite size corrections to the partition function are uniquely fixed only by the two (three) low energy constants in the ϵ- (p-) expansion not only to the leading order $1/L$ but also to the next leading $1/L^2$[1]. They are the magnetization Σ and the helicity modulus Υ (and an additional constant for the p-expansion) in infinite volume. The helicity modulus is a quantity associated with the response to the distortion of the direction of the spontaneous symmetry breaking [14]. An increment of the free energy per volume due to the distortion is given by $\Delta f = \Upsilon(\Delta\epsilon)^2/2$, where $\Delta\epsilon$ stands for the gradient of the twist in one spatial direction . The equivalence between the helicity modulus and the Goldstone boson decay constant F is shown in ref.[1]; $\Upsilon = F^2$. A numerical study of the finite size behavior of the system would then provide these constants and their associated critical indices in a high accuracy. To the $d = 4$ O(4) scalar model [15] [16] [17] and the $d = 3$ classical Heisenberg model [18] the chiral perturbation theory has successfully been applied.

As stated above, each expansion has its own characteristic region, which manifests itself in the external source plane. It is then worthwhile to have a careful look at where each of them is located and whether the two overlaps or not. The authors of the paper [15] have addressed this issue. We shall study this aspect in more detail.

This paper is organized as follows. In section 2 we define the model and fix the notations. We summarize the formulae of the ϵ- and p- expansions for the magnetization, the susceptibilities and the two point correlation functions. In section 3 we present the results of our numerical simulations based upon the cluster algorithm. Section 4 is devoted to conclusions and discussion.

2. The XY model and formulae of the chiral perturbation theory in 3 dimensions

The $O(2)$ linear σ model coupled with a constant external source j is defined in the continuum euclidean space time as

$$\mathcal{L} = \frac{1}{2}(\partial_\mu \phi^i(x))^2 + \frac{1}{2}m^2(\phi^i(x))^2 + \lambda((\phi^i(x))^2)^2 - j\phi^0(x) \tag{2.1}$$

where $\phi(x)$ is a two component real vector (i= 0 and 1), and m and λ stand for the bare mass and the bare quartic coupling constant, respectively. The external source has only $i = 0$ component. To put the model on a lattice, one rescales all the dimensionful quantities by a lattice constant a, and conventionally uses three dimensionless parameters; the quartic coupling parameter λ_{lat}, the hopping parameter κ and the external source J. The lattice action is

$$S = -\kappa \sum_{n,\mu,i} \varphi_n^i \varphi_{n+\mu}^i + \sum_{n,i} \varphi_n^i \varphi_n^i + \lambda_{lat} \sum_n \Big(\sum_i \varphi_n^i \varphi_n^i - 1 \Big)^2 - J \sum_n \varphi_n^0 \tag{2.2}$$

where φ_n^i is the dimensionless field $\varphi_n^i = (1/\sqrt{\kappa})\ \phi^i(na)a^{d/2-1}$ sitting at site n and μ is a unit vector of the μ direction. The lattice parameters are related to those of continuum in such a way as $(ma)^2 = (2 - 4\lambda_{lat})/\kappa - 2d$, $\lambda a^{4-d} = \lambda_{lat}/\kappa^2$, $ja^{1+d/2} = J/\sqrt{\kappa}$. For $\lambda_{lat} = \infty$, the radial mode of φ_n is frozen to unity, and the action reduces to that of the O(2) non-linear sigma model or the XY model.

Our aim in the present paper is to compute, in the $d = 3$ XY model, two low energy constants in infinite volume, which are the magnetization Σ

$$\lim_{j\to 0} \lim_{V\to\infty} \langle \phi^0 \rangle_{j,V} = \Sigma \tag{2.3}$$

and the helicity modulus (or the Goldstone boson decay constant) F appearing in the following equation

$$\int dx\ e^{ipx} \langle A_\mu(x) A_\nu(0) \rangle_{j=0, V=\infty} = \delta^{\mu\nu} \frac{iF^2}{p^2} + \cdots \tag{2.4}$$

where $A_\mu = \phi^0 \partial_\mu \phi^1 - \phi^1 \partial_\mu \phi^0$. The quantity $\langle \phi^0 \rangle_{j,V}$ is the expectation value of ϕ^0 in a three dimensional box with finite volume V in the presence of the external source j.

In $d = 3$, all the formulae of the chiral perturbation theory are basically fixed only by these two low energy constants to $O(1/L^2)$. It is unlike the four dimensional models where a few additional constants are necessary[1]. In the following, we summarize the formulae of the chiral perturbation theory necessary to our analysis of finite size effects on the magnetization, the susceptibility and the two point functions. Detail about the formulae is found in ref.[1] for the ϵ-expansion and in ref.[19] for the p-expansion.

In order for the chiral perturbation theory to be effective, the Goldstone modes should be important at long distances. That is to say, finite size effects from the massive component with a mass m_σ must be negligible compared to the Goldstone boson mass m_π, i.e., $m_\sigma / m_\pi \gg 1$. Assuming the dominance of the Goldstone modes two manners of expansions are possible depending upon what quantities are fixed in the expansions[1]. One is called ϵ-expansion, in which the total magnetic energy $u_0 = \Sigma j L^d$ is fixed to $O(L^0)$, and another is p-expansion where $v = \Sigma j L^2 / F^2$ is fixed to $O(L^0)$. The latter gives $j \sim L^{-2}$, while the former does $j \sim 1/L^d$. By using the Goldstone mass m_π, which is given by $m_\pi^2 = \Sigma j / F^2$, or the corresponding correlation length $\xi_\pi = 1/m_\pi$, the domain is characterized by $m_\pi L \lesssim 1 \quad (\xi_\pi \gtrsim L)$ for the ϵ-expansion and by $m_\pi L \gtrsim 1 \quad (\xi_\pi \lesssim L)$ for the p-expansion. Since $m_\pi L = \sqrt{\Sigma j} L / F \lesssim 1$ yields $j \lesssim F^2 / \Sigma L^2 = \text{const.}$ for a fixed κ and L, one expects in the j space that the ϵ- (p-) expansion holds in the smaller (larger) j domain. As one moves κ, each of the regions shifts. In the vicinity of the critical point κ_c, Σ and F behave as $\Sigma \sim (\kappa - \kappa_c)^{\nu(1+\eta)/2}$ and $F \sim (\kappa - \kappa_c)^{\nu/2}$, respectively. One hence expects that $m_\pi L = \sqrt{\Sigma j} L / F \approx 1$ leads to $j \sim F^2 / \Sigma \sim (\kappa - \kappa_c)^{\nu(1-\eta)}$ for a fixed L. Therefore the domain for the ϵ-expansion shrinks as κ approaches κ_c from above, since the index η, anomalous dimension of the field, is smaller than unity for the model in consideration. It is one of our motivations to locate the region of each expansion in the j space. It is also interesting to study to what extent each region is extended beyond the point where $m_\pi L \approx 1$. This is another motivation of our work. In the present paper we shall look into these aspects in detail.

All the formulae in this section are of order $O(L^{-2})$. Hereafter we call the direction of the external source ($i = 0$) the longitudinal direction and another direction (i=1) the transverse one. They are denoted as $\|$ and $\perp$, respectively. We work only with finite volume and finite j, and drop, for simplicity, the suffices j and V from $\langle\phi^0\rangle_{j,V}$. As an expansion parameter we use $\alpha(= 1/F^2L)$.

2.1. ϵ-expansion

The magnetization in the direction of an external source is

$$\langle\phi^0\rangle = \Sigma u[\rho_1\eta + 2\rho_2\alpha^2], \tag{2.5}$$

where $u = \rho_1\Sigma jV$, and ρ_1 and ρ_2 are quantities depending on the shape of the box;

$$\begin{aligned} \rho_1 &= 1 + \frac{1}{2}\beta_1\alpha + \frac{1}{8}(\beta_1^2 - 2\beta_2)\alpha^2 \\ \rho_2 &= \frac{1}{4}\beta_2. \end{aligned} \tag{2.6}$$

For a three dimensional symmetric box, $\beta_1 = 0.225785$ and $\beta_2 = 0.010608$. The quantity η in (2.5) is given by the modified Bessel's functions $I_n(x)$ as

$$\eta = \frac{1}{u}\frac{I_1(u)}{I_0(u)}. \tag{2.7}$$

Two point correlation functions are defined as

$$G^{ij}(t) = \frac{1}{L^2}\sum_{\mathbf{n}}\langle\phi^i(\mathbf{n},t)\phi^j(\mathbf{0},0)\rangle \tag{2.8}$$

where the summation is taken over in spatial 2-volume at fixed "time" t ($0 \leq t < L$). We consider two correlation functions; the longitudinal and transverse ones;

$$G^\epsilon_\|(\tau) = G^{00}(t), \qquad G^\epsilon_\perp(\tau) = G^{11}(t), \tag{2.9}$$

where $\tau = t/L$ and $0 \leq \tau < 1$. In the ϵ-expansion each correlation function takes the following form

$$G^\epsilon_\|(\tau) \equiv a_\| + b_\| h_1(\tau) + c_\| h_2(\tau) + d_\| h_3(\tau), \tag{2.10}$$

$$G^\epsilon_\perp(\tau) \equiv a_\perp + b_\perp h_1(\tau) + c_\perp h_2(\tau) + d_\perp h_3(\tau), \tag{2.11}$$

where coefficients $a_\parallel, b_\parallel, c_\parallel$ and $d_\parallel$ and their transverse counterparts are expanded in powers of α. The τ dependence enters through the following kinematic functions

$$\begin{aligned} h_1(\tau) &= \frac{1}{2}\Big((\tau - \frac{1}{2})^2 - \frac{1}{12}\Big) \\ h_2(\tau) &= \frac{1}{24}\Big(\tau^2(1-\tau)^2 - \frac{1}{30}\Big) \\ h_3(\tau) &= h_1(\tau)^2 + \sum_{\mathbf{n}}{}' \frac{\cosh\big(q_{\mathbf{n}}(\tau - 1/2)\big)}{2q_{\mathbf{n}}\sinh(q_n/2)} - \beta_2. \end{aligned} \tag{2.12}$$

The summation on the r.h.s. of $h_3(\tau)$ is taken over all integers (n_1, n_2) except for $\mathbf{n} = (0,0)$, and $q_{\mathbf{n}}$ stands for $q_{\mathbf{n}} = 2\pi\sqrt{n_1^2 + n_2^2}$. The coefficients a, b, c and d for the longitudinal correlation function in (2.10) are given by

$$\begin{aligned} a_\parallel &= \Sigma^2\left\{\rho_1^2(1-\eta) + 2\rho_2(1+2u^2\eta)\alpha^2\right\} \\ b_\parallel &= \Sigma^2\rho_1^2\eta\alpha \\ c_\parallel &= \Sigma^2(1-2\eta)\alpha^2 \\ d_\parallel &= \Sigma^2(1-\eta)\alpha^2/2, \end{aligned} \tag{2.13}$$

while the transverse ones in (2.11) are given by

$$\begin{aligned} a_\perp &= \Sigma^2\left\{\rho_1^2\eta + 2\rho_2\alpha^2\right\} \\ b_\perp &= \Sigma^2\rho_1^2(1-\eta)\alpha \\ c_\perp &= \Sigma^2\left(-1 + (2+u^2)\eta\right)\alpha^2 \\ d_\perp &= \Sigma^2\eta\alpha^2/2. \end{aligned} \tag{2.14}$$

Note that a, b, c and d are of $O(1), O(\alpha), O(\alpha^2)$ and $O(\alpha^2)$, respectively, for both the cases. We use these correlation functions to extract the low energy constants. In addition to these, we find that the scalar product correlation function is also practically of much use;

$$\begin{aligned} G_s^\epsilon(\tau) &= \frac{1}{L^2}\sum_{\mathbf{n}}\langle\phi(\mathbf{n}, L\tau)\cdot\phi(\mathbf{0}, 0)\rangle \\ &= G_\parallel^\epsilon(\tau) + G_\perp^\epsilon(\tau) \\ &= a_s + b_s h_1(\tau) + c_s h_2(\tau) + d_s h_3(\tau), \end{aligned} \tag{2.15}$$

where the coefficients a_s etc. are given by

$$\begin{aligned} a_s &= \Sigma^2\left\{\rho_1^2 + 4\rho_2(1+u^2\eta)\alpha^2\right\} \\ b_s &= \Sigma^2\rho_1^2\alpha \\ c_s &= \Sigma^2u^2\eta\alpha^2 \\ d_s &= \Sigma^2\alpha^2/2. \end{aligned} \tag{2.16}$$

The longitudinal susceptibility is calculated from it's correlation function

$$\chi_{\parallel} = \sum_{n} \left(\langle \phi^0(n)\phi^0(0) \rangle - \langle \phi^0 \rangle^2 \right), \tag{2.17}$$

and it takes the form

$$\chi_{\parallel} = \Sigma^2 V \left[\rho_1^2 \{ (1-\eta) - u^2\eta^2 \} + 2\rho_2\alpha^2 \right]. \tag{2.18}$$

2.2. p-expansion

In the p-expansion to $O(L^{-2})$ a low energy constant k_0 gets involved in addition to Σ and F for the magnetization and the susceptibilities.

The magnetization reads

$$\begin{aligned} \langle \phi^0 \rangle =& \Sigma \left\{ 1 + \frac{1}{8}\alpha\zeta^{1/2} + k_0\alpha^2\zeta - \frac{1}{2}\alpha\big[1 + \frac{3}{16\pi}\alpha\zeta^{1/2}\big] g_1(\zeta_p) \right. \\ & \left. + \frac{1}{8}\alpha^2 g_2(\zeta)\big[g_1(\zeta) - \zeta g_2(\zeta)\big] \right\}, \end{aligned} \tag{2.19}$$

where $\zeta = (m_\pi L)^2$ ($m_\pi^2 = \Sigma j/F^2$) , and ζ_p is

$$\zeta_p = \zeta\big(1 + \frac{1}{8\pi}\alpha\zeta^{1/2}\big). \tag{2.20}$$

The function $g_n(\zeta)(n = 0, 1, 2, ...)$ are defined by

$$g_0(\zeta) = -\ln\zeta - \frac{\zeta^{3/2}}{4\pi} - \sum_{n=0}^{\infty} \frac{\beta_n}{n!}\zeta^n \tag{2.21}$$

$$g_{n+1}(\zeta) = -\frac{d}{d\zeta}\ g_n(\zeta). \tag{2.22}$$

The correlation functions defined in (2.9) and (2.15) take the forms

$$G^p_{\parallel}(\tau) = \langle \phi^0 \rangle^2 + \frac{1}{2}\Sigma^2\alpha^2\bar{h}_2(\tau) \tag{2.23}$$
$$G^p_{\perp}(\tau) = Z_v\alpha\bar{h}_1(\tau), \tag{2.24}$$

where Z_v is the wave function renormalization constant in a finite box with the form

$$Z_v = \Sigma^2 \left[1 + \frac{1}{4\pi}\alpha\zeta^{1/2} - g_1(\zeta)\alpha \right]. \tag{2.25}$$

The kinematic functions $\bar{h}_1(\tau)$ and $\bar{h}_2(\tau)$ involved in the p-expansion are

$$\begin{aligned}\bar{h}_1(\tau) &= \bar{h}(\tau, \zeta_v)\\ \bar{h}_2(\tau) &= \sum_{\mathbf{n}} \bar{h}^2(\tau, \zeta + 4\pi^2 |\mathbf{n}|^2)\end{aligned}$$

where $\bar{h}$ on the r.h.s. is given by

$$\bar{h}(\tau, \zeta) = \frac{1}{2\sqrt{\zeta}} \frac{\cosh\left(\sqrt{\zeta}(\tau - 1/2)\right)}{\sinh \sqrt{\zeta}/2}$$

and ζ_v is

$$\zeta_v = \zeta_p \left[1 - \frac{1}{2} g_1(\zeta)\alpha\right]. \tag{2.26}$$

The transverse correlation function has a normal form of massive scalar propagator to $O(\alpha)$, while the connected part of the longitudinal one (2.23) is $O(\alpha^2)$. We also consider the scalar product correlation function

$$G_s^p(\tau) = G_{\parallel}^p(\tau) + G_{\perp}^p(\tau). \tag{2.27}$$

As in the ϵ-expansion, $G_s^p(\tau)$ is of practical use.

The susceptibility in (2.17) in terms of p-expansion reads

$$\begin{aligned}\chi_{\parallel} = \Sigma V \alpha \Bigg\{ &\frac{1}{16\pi} \alpha \zeta^{1/2} + k_0 \alpha^2 \\ &- \frac{1}{2}\alpha \left[-g_2(\zeta_p) - \frac{3}{32\pi} \alpha \zeta^{1/2} \left(g_1(\zeta_p) + 2(1+\zeta) g_2(\zeta_p) \right) \right] \\ &+ \frac{1}{4} \alpha^2 \left[-2 g_1 g_2 + \zeta ({g_2}^2 + g_1 g_3) \right] \Bigg\}.\end{aligned} \tag{2.28}$$

3. Numerical simulations

We employ, to generate configurations, the Wolff's single cluster algorithm [20] and its modification in the case of presence of an external source[18]. The lattice shape which we take is a symmetric box with a volume $V = L^3$, and the size of the box ranges from $L = 32$ to $L = 64$. The $d = 3$ dimensional XY model is known to have a second order phase transition at $\kappa_c = 0.45420(2)$[9]. We calculate at κ larger than κ_c, and choose two κ values κ=0.462 and 0.47 for main calculations of the low energy constants, and several more for obtaining the critical indices. The magnitudes of the external source changes from $J = 0.0$ to $J = 5.0 \times 10^{-4}$. In terms of continuum external source, which depends on κ, j ranges from 0 to 7.29 $\times 10^{-4}$ for, say, $\kappa = 0.47$. We make measurements at each 5 updatings with typical number of configurations for measurements ranging from about 20,000 to 40,000. The statistical errors are estimated by using the blocking and the bootstrap methods. We use the program system SALS [21] for the least square fitting of the data to the formulae.

We extracted Σ and F from three types of correlation functions in each of the ϵ- and p- expansions. We looked at the behaviors of each of the extracted values by varying J. We also observed the magnetization and the susceptibility, and compared the results with the formulae of the chiral perturbation theory. Main results are in order.

(1) We found, as expected from the arguments in the Sec. 2, that the ϵ-expansion provides good results in the small J region, while the p-expansion does so in the larger J region. We identified where the region of the validity for each of the two manners of expansions is located.

(2) The scalar product correlation functions provide stable results for the two constants.

(3) Upon varying the size of the lattice, which is sensitive to the region of the validity, we observed a significant change of the behavior for the p-expansion. It is consistent with the arguments concerning m_π and m_σ.

(4) The magnetization shows a clear crossover behavior between the two expansions as a function of J. The longitudinal susceptibility turns out too poor to address the region of the validity.

(5) We calculated the critical indices associated with the two constants. The results are consistent with other references.

In the following we shall discuss the results in detail.

3.1. Correlation functions

In order to extract $\Sigma(\kappa)$ and $F(\kappa)$ from the correlation functions, we fit to the formulae (2.10), (2.11) and (2.15) for the ϵ-expansion and to (2.23), (2.24) and (2.27) for the p-expansion for each j at fixed κ. We use hereafter the notation $\Sigma_{(\epsilon,p),(||,\perp,s)}$ for the value of $\Sigma(\kappa)$ obtained from each type of correlation functions in each expansions. Similar notations are used also for F. All the extracted values of Σ and F are listed in Table I – V. In what follows we discuss the stability of the extracted results and the region of the validity of each of the expansions by comparing the values in Tables. If the chiral perturbation theory works, the extracted values should be independent of J, and all of the values $\Sigma_{(\epsilon,p),(||,\perp,s)}$ ($F_{(\epsilon,p),(||,\perp,s)}$) should agree.

Results of $L = 32$ lattice ($\kappa = 0.47$)

In Figs. 1 and 2 we show the behaviors of the obtained $\Sigma(\kappa)$ and $F(\kappa)$ v.s. the magnitude of the external source J at $L = 32$ for κ=0.47. In Fig. 1 we see that the ϵ-expansion provides the consistent result for Σ within errors for two types of correlation functions, i.e., longitudinal one $G^{\epsilon}_{||}(\tau)$ and transverse one $G^{\epsilon}_{\perp}(\tau)$, in the whole J range in consideration. The p-expansion, on the other hand, is out of validity in the smaller J region, $J \lesssim 2.0 \times 10^{-4}$ (Fig. 1). At larger J values, the transverse one $\Sigma_{p,\perp}$ agrees with Σ of the ϵ-expansion. We hence observe that an overlap of the two expansions takes place at $J \gtrsim 2.0 \times 10^{-4}$.

The result of the longitudinal p-expansion is not included in the figure. Fittings according to this type of expansion turn out invalid in the whole J range. This may be due to the fact that τ dependence appears only at $O(\alpha^2)$ unlike the all other correlation functions of $O(\alpha)$, and that the data would be too noisy to extract the Σ. This feature applies also to F and to different volumes. We then drop the result of the longitudinal p-expansion throughout the paper.

Fig. 2 shows F v.s. J. Both of $F_{\epsilon,||}$ and $F_{\epsilon,\perp}$ agree within errors in the small J region ($J \lesssim 2.0 \times 10^{-4}$), while $F_{\epsilon,||}$ and $F_{\epsilon,\perp}$ split from each other for larger J ($J \gtrsim 2.0 \times 10^{-4}$). This indicates that the boundary of the two domains where the ϵ-expansion is valid and invalid is located at $J \approx 2.0 \times 10^{-4}$. Fig. 2 also shows the behaviors of F for the p-expansion. Similarly to Σ, the p-expansion does not give a reasonable result in the smaller J region, but agree with F of ϵ-expansion at $J \gtrsim 2.0 \sim 3.0 \times 10^{-4}$.

The lowest value of the overlapping region for Σ and F is consistent with what one naively expects from the argument concerning the Goldstone mass (Sec. 2); the two expansions coincide at a point J which is determined by the relation $M_\pi L = \sqrt{\Sigma j}L/F \approx 1$. Taking the values $\Sigma(0.47) = 0.2581(1)$, $F(0.47) = 0.286(1)$ and $L = 32$ for $\kappa = 0.47$, it yields 2.1×10^{-4}, which is in good agreement with the observed value. Note that the errors of F are about five times larger than those of Σ at whole κ's and J's in consideration.

Results of $L = 32$ lattice ($\kappa = 0.462$)

Similar behaviors are seen for the data of $\kappa = 0.462$ and $L = 32$ (Fig. 3). However, $\Sigma_{\epsilon,||}$ and $\Sigma_{\epsilon,\perp}$ agree only at small J values ($J \lesssim 2.0 \times 10^{-4}$) compared to $\kappa = 0.47$ (Fig. 1). This is in fact what is expected from the condition giving the region of the expansion $M_\pi L \lesssim 1$, since the region of the ϵ-expansion shrinks according to $j \lesssim (\kappa - \ \kappa_c)^{\nu(1-\eta)}$ as

κ approaches $\kappa_c (\kappa_c = 0.4546)$ as stated in Sec. 2. We see that this behavior becomes even clearer for F (see Table II).

Fig. 3 also shows the behaviors of the p-expansion. The value $\Sigma_{p,\perp}$ seems reasonable only in the limited intermediate region around $J \approx 2.0 \times 10^{-4}$. In larger J region the p-expansion becomes invalid unlike the case of $\kappa = 0.47$. The reason for that comes from the mass m_σ of the massive particle; as stated in Sec. 2, m_σ must be large enough $m_\sigma/m_\pi \gg 1$. In the case of $\kappa = 0.47$ we obtained $m_\sigma \approx 0.41$, which gives the ratio m_σ/m_π ranging from 20.5 to 10.1 as J changes from 1.0×10^{-4} to 5.0×10^{-4}. m_σ is then heavy enough for the chiral perturbation to apply at $\kappa = 0.47$.

For $\kappa = 0.462$, on the other hand, we obtained smaller value $m_\sigma = 0.3$, which yields m_σ/m_π ranging from 12.5 to 5.5 in the same J range. The authors of the paper [15] took $m_\sigma/m_\pi \gtrsim 10$ as a criterion. If we employ the same value, it provides an upper bound of J, $J \lesssim 1.5 \times 10^{-4}$, on the region of the validity of the chiral perturbation theory. Combining the condition $m_\pi L \gtrsim 1$, which gives a lower bound of J, $J \gtrsim 1.66 \times 10^{-4}$, on the region of the p-expansion, one observes that there is no region for the validity of the p-expansion. If $m_\sigma L \gtrsim 7.5$ is adopted instead of 10, however, the upper bound shifts to $J = 2.7 \times 10^{-4}$. Although these bounds should not be taken strictly, it indicates that the p-expansion is expected to apply to no or only the narrow J region around $J = 1.6 \sim 2.5 \times 10^{-4}$. In other words, the "window" for the p-expansion is almost closed or open only slightly. The results of our fittings are in good agreement with this inference (Fig. 3).

Scalar product correlation function

Apart from the longitudinal and transverse correlation functions, we made also use of the scalar product correlation functions (2.15) and (2.27). During our fitting procedure we came to notice that the scalar product correlation functions are good correlators which provide stable fitting results. In particular, the ϵ-expansion works very well.

In Fig. 4 we show the results of Σ for both of the ϵ- and p-expansions at $L = 32$ for $\kappa = 0.47$ and 0.462. For both κ values $\Sigma_{\epsilon,s}$ looks almost independent of J in the whole J range, and therefore it provides reliable result. This is the reason why we indicated the value $\Sigma_{\epsilon,s}$ in Figs. 1 and 3 by the arrow as a reference. In the region of validity of the ϵ-expansion at each κ, $\Sigma_{\epsilon,s}$ is consistent with $\Sigma_{\epsilon,\parallel}$ and $\Sigma_{\epsilon,\perp}$. Compared to the other two, $\Sigma_{\epsilon,s}$ is much stable.

The value $\Sigma_{p,s}$, on the other hand, vary as J moves. For $\kappa = 0.47$ it monotonically approaches $\Sigma_{\epsilon,s}$ as J increases, and gives consistent result at $J \gtrsim 3.0 \times 10^{-4}$. For $\kappa = 0.462$, on the other hand, $\Sigma_{p,s}$ never agrees with $\Sigma_{\epsilon,s}$ even in the larger J region. The scalar product correlation functions supports more clearly, than do the longitudinal and the transverse correlation functions, the inference based upon m_σ and m_π about the location of the boundary between the two expansions. Similar behaviors are seen also for F as shown in Fig. 5.

Volume dependence

Let us turn to the volume dependence. The extracted values of Σ and F for $L = 48$ are listed in Tables III and IV . The average values for $L = 48$ are consistent with those for $L = 32$ in the regions of the validity of each of the expansions.

When one increases the volume, J value corresponding to the condition $m_\pi L \approx 1$ decreases as $J \propto 1/L^2$, while the ratio m_σ/m_π is independent of L. It is therefore expected that the "window" for the p-expansion becomes wider as L increases. It is then interesting if one actually sees this behavior by simulations. For $L = 32$ at $\kappa = 0.462$, we have seen that the "window" is almost closed. Fig. 6 shows $\Sigma_{\epsilon,s}$ and $\Sigma_{p,s}$ for $L = 48$ at $\kappa = 0.462$ obtained from the scalar correlation functions. The value $\Sigma_{p,s}$ agrees with $\Sigma_{\epsilon,s}$ only around $J = 2.0 \times 10^{-4}$, which is regarded as an evidence of slightly opening "window". It is in good contrast with the behavior of $\Sigma(\kappa = 0.462)$ in Fig. 4. Similar behavior is found also for F as shown in Figs. 5 and 7.

In the absence of J we calculated Σ and F at $L = 64$, and compared them with those of $L = 32$ and 48. As seen in Table V the results of $\Sigma_{\epsilon,s}$ and $F_{\epsilon,s}$ are consistent within errors.

3.2. Magnetization and susceptibility

We calculate the magnetization for the ϵ-expansion (2.5) for the p-expansion (2.19). Rather than fitting (2.5) and (2.18) to the data to extract Σ and F, we put Σ and F into eqs. (2.5) and (2.19) and compare them with those of direct measurements of $\langle \varphi^0 \rangle$. Here we use the values of Σ and F obtained from the correlation functions at each κ, $\kappa = 0.462$ and $\kappa = 0.47$, in the previous subsection. In the p-expansion, an additional low energy constant k_0 is involved as mentioned before. To determine k_0, we match the curve (2.19) to the data at some J.

Fig. 8 shows the results for $\kappa = 0.462$ and 0.47 at $L = 32$. The constant k_0 is fixed at $J = 2.0 \times 10^{-4}$ for $\kappa = 0.462$ and at $J = 3.0 \times 10^{-4}$ for $\kappa = 0.47$. Solid line in the figure shows the curve (2.5) and dotted line is (2.19). We see a good agreement and observe a clear crossover between the ϵ- and the p-expansions. The location of the crossover between both the expansions is consistent with the prediction $m_\pi L \approx 1$.

The results of $L = 48$ are shown in Table VI. The values obtained from the p-expansion formula (2.19) are $\langle \varphi^0 \rangle = 0.201$ at $J = 0.5 \times 10^{-4}$, 0.2934 at $J = 2.0 \times 10^{-4}$ and 0.3083 at $J = 3.0 \times 10^{-4}$ for $\kappa = 0.462$. The two of them ($J = 0.5 \times 10^{-4}$ and 2.0×10^{-4}) are consistent with the numerical result within errors. Another one ($J = 3.0 \times 10^{-4}$) seems to deviate slightly from the data. For $\kappa = 0.47$, the values of $\langle \varphi^0 \rangle$ read 0.279 at $J = 0.5 \times 10^{-4}$, 0.3357 at $J = 1.0 \times 10^{-4}$ and 0.3776 at $J = 3.0 \times 10^{-4}$, respectively. In the similar manner to $\kappa = 0.462$ only the two points ($J = 0.5 \times 10^{-4}$ and 1.0×10^{-4}) out of three are in good agreement with the data within errors. In any case, theoretical predictions are not inconsistent with the measurements.

Let us turn to the longitudinal susceptibility $\chi_{||}$. Fig. 9 shows the J dependence of $\chi_{||}$ for $L = 32$ at $\kappa = 0.462$ and 0.47. The solid (dotted) lines correspond to (2.18)((2.28)). For each of the fixed κ, $\chi_{||}$ shows a crossover at $J \approx 2.0 \times 10^{-4}$ if the ϵ- (p-) expansion is valid in the smaller (larger) J region. In the actual measurements we are not able to observe such a clear crossover.

As to the relation between the lines for the two κ's we can read off qualitative difference as follows. For smaller J ($J \lesssim 2.0 \times 10^{-4}$), the values of $\chi_{||}(\kappa = 0.462)$ are lower than $\chi_{||}(\kappa = 0.47)$, while in larger J region $\chi_{||}(\kappa = 0.462)$ becomes higher than $\chi_{||}(\kappa = 0.47)$. This property is successfully seen in the direct measurements. Quantitatively, however, there are some inconsistencies between the theoretical predictions and the numerical data.

The J dependence of $\chi_{||}$ in the case of $L = 48$ is shown in Table VII. The situation is the same as in the case of $L = 32$.

3.3. Critical index

The critical indices β and ν are defined by

$$\begin{aligned} \Sigma(\kappa) &\sim (\kappa - \kappa_c)^{\beta} \\ F(\kappa) &\sim (\kappa - \kappa_c)^{\nu/2} \end{aligned} \tag{3.1}$$

in 3 dimensions[1]. To extract β and ν we make use of the values of Σ and F in infinite volume obtained from the previous analysis. We fit to (3.1) the data at five κ points ($\kappa = 0.46, 0.462, 0.464, 0.466, 0.47$). The results are

$$\kappa_c = 0.4546(5) \tag{3.2}$$

for the critical coupling

$$\begin{aligned} \beta &= 0.321(17) \\ \nu &= 0.66(6) \end{aligned} \tag{3.3}$$

for the indices. They are consistent with other references[6][8][9][10][11][12][13].

4. Conclusions and discussion

We applied the chiral perturbation theory à la Hasenfratz and Leutwyler to the $d = 3$ XY model in order to calculate the two low energy constants. They are the magnetization Σ and the helicity modulus F (or Goldstone boson coupling) in infinite volume. In the theory, two manners of the expansions are involved. One is the ϵ-expansion, which is valid in the region where $m_\pi L \lesssim 1$, and another is the p-expansion, where $m_\pi L \gtrsim 1$. On $L = 32$, 48 and 64 lattices, we fitted the formulae of the correlation functions to the Monte Carlo data. All the values of Σ and F extracted in each of the regions of the validity are consistent and volume independent within errors.

We are also particularly concerned with the region of the validity of the two expansions. As far as the two κ values are concerned, the lower boundary of the p-expansion is basically located at the region where $m_\pi L \approx 1$ holds. On the other hand, the ϵ-expansion stretches, for some cases, beyond the point $M_\pi L \approx 1$ to some extent than expected. The similar behavior was also observed in ref.[15]. Apart from the condition for $m_\pi L$, the mass m_σ of the massive particle puts a constraint on the validity of the chiral perturbation theory. As expected from these conditions, we have observed the significant difference of the behaviors of Σ and F v.s. the external source J for the two different κ values.

We found that the scalar product correlation functions are better correlators than the longitudinal and transverse correlation functions. Particularly the ϵ-expansion provides quite stable estimations of Σ and F. By use of it the overlapping of the validity of both the expansions is clearly seen. The reasons for the stability are in order. The coefficient $b_s = \Sigma^2 \rho_1^2 \alpha$ in (2.16) is independent of j, unlike the longitudinal $b_\parallel$ in (2.13) and the transverse counterparts $b_\perp$ in (2.14), in which j dependence appears through $u = \rho_1 \Sigma j V$. To $O(\alpha)$, therefore, no response of G_s^ϵ to the variation of j appears. It is then expected that $\Sigma_{\epsilon,s}$ and $F_{\epsilon,s}$ are extracted independently of j. This is one of the reasons for the stability *. However for $J \gtrsim 3.0 \times 10^{-4}$, Σ and F deviate from their stable values, i.e., in

---

* The fact that b_s is independent of j to $O(\alpha)$ applies only to $N = 2$ for the $O(N)$ model.

this J region the contribution from $O(\alpha^2)$ would be responsible for the stability. In order to have a look at its effect, we compared the two ways of fitting of G_s^ϵ using the formulae to $O(\alpha)$ and to $O(\alpha^2)$. We found that in the small j region ($J \lesssim 3.0 \times 10^{-4}$) the results of the two fittings are in agreement with each other within errors, while in the larger region the significant discrepancy appears. (The relative difference of the two fits is approximately 4% for $F(\kappa = 0.47)$ at $J = 5.0 \times 10^{-4}$) One then sees that the correction of $O(\alpha^2)$ plays a significant role to the stability in the larger J region.

The magnetization $\langle \varphi^0 \rangle$ and the susceptibility $\chi_{||}$ are fitted by use of the values of Σ and F obtained by the correlation functions. The consistency was checked. The magnetization is well fitted by the ϵ-expansion in the smaller J region and by the p-expansion in the larger one. A crossover between both the expansions in the J space was observed, and its location is consistent with the prediction $m_\pi L \approx 1$. The susceptibility turns out too poor in precision to address the issue about the validity of the expansions.

We calculated the critical indices associated with Σ and F, and obtained the values consistent with other references. However we have not reached the precision as high as that of ref.'s [8] and [9], which is based upon the phenomenological renormalization group. This may be due to the fact that the chiral perturbation theory becomes hard to apply as it is. Because, as one approaches the critical point, the mass m_σ of the massive particle gets smaller and the ratio m_σ/m_π accordingly becomes small. In addition, the expansion parameter $\alpha = 1/F^2L$ becomes large.

A few words for the values of the constant F. We compared the value of Υ calculated from F with the one in the available references. Our values** $\Upsilon = F^2 = 0.0515(14)$ at $\kappa = 0.462$ and $0.042(2)$ at $\kappa = 0.460$ in infinite volume come slightly below the curves in the figures of refs. [6] and [8], in which the lattice size L is at most 48. It is reasonable since in their data the values monotonically decrease as L grows.

** Note that F^2/κ corresponds to the helicity modulus in their literatures.

Acknowledgment

We thank M. Imachi for a careful reading of the manuscript. We are grateful to M.Imachi and T. Kashiwa for encouragement and useful discussions, and to the members of the high energy theory groups in Kyushu University and Saga University for discussions. The numerical simulation was performed on FACOM M-1800/20 at RCNP, Osaka university.

References

[1] P. Hasenfratz and H. Leutwyler , Nucl. Phys. **B343**, 241 (1990)

[2] J. Gasser and H. Leutwyler, Ann. Phys. **158**,142 (1984)

[3] M. E. Fisher and V. Privman, Phys. Rev. **B32**, 447 (1985)

[4] E. Brézin and J. Zinn-Justin, Nucl. Phys. **B257**[FS14], 867 (1985)

[5] T. Ohta and D. Jasnow, Phys. Rev. **B20**, 139 (1979)

[6] Y-H Li and S. Teitel, Phys. Rev. **B40**, 9122 (1989)

[7] M. Hasenbusch and S.Meyer, Phys. Lett. **B241**, 238 (1990)

[8] W. Janke, Phys. Lett. **A148**, 306 (1990)

[9] A. P. Gottlob, M. Hasenbusch and S. Meyer, Nucl. Phys. **B**(Proc. Suppl.) **30**, 838 (1993) ; A. P. Gottlob and M. Hasenbusch, (unpublished)

[10] J.C. Le Guillou and J. Zinn-Justin, Phys. Rev. **B21**, 3976 (1980)

[11] M. Ferer, M. A. Moore and M. Wortis, Phys. Rev. **B8**, 5205 (1973)

[12] J. Adler, C. Holm and W. Janke, (unpublished)

[13] P. Butera, M. Comi and A. J. Guttman, Phys. Rev. **B48**,13987 (1993)

[14] M.E. Fisher, M.N. Barber and D. Jasnow, Phys. Rev. **A8**,1111 (1973)

[15] A. Hasenfratz, K. Jansen, J. Jersák, H.A. Kastrup, C.B. Lang, H. Leutwyler and T. Neuhaus, Nucl. Phys. **B356**, 332 (1991)

[16] M. Göckeler and H. Leutwyler, Phys. Lett. **B253**, 193 (1991)

[17] M. Göckeler, K. Jansen and T. Neuhaus, Phys. Lett. **B273**, 450 (1991)

[18] I. Dimitrović, P. Hasenfratz, J. Nager and F. Niedermayer, Nucl. Phys. **B350**, 893 (1991)

[19] M. Göckeler and H. Leutwyler, Nucl. Phys. **B361**, 392 (1991)

[20] U. Wolff, Phys. Rev. Lett. **62**, 361 (1989)

[21] T.Nakagawa and Y.Oyanagi, ‘Program System SALS for Nonlinear Least-Squares Fitting in Experimental Sciences’, in Recent Developmetnt in Statistical Infernce and Data Analysis, North-Holland(1980)

Table Captions

Table I	Σ and F for $\kappa = 0.47$ and $L = 32$. The symbol *** indicates the point where the p-expansion is beyond the applicability. The symbol ### shows that we failed to fit the formulae. The same symbols are used in the other tables.
Table II	Σ and F for $\kappa = 0.462$ and $L = 32$.
Table III	Σ and F for $\kappa = 0.47$ and $L = 48$.
Table IV	Σ and F for $\kappa = 0.462$ and $L = 48$.
Table V	Σ and F for $L = 64$ and $J = 0.0$.
Table VI	$\langle \varphi^0 \rangle$ v.s. J for $L = 32$ and $L = 48$. By the symbol %%% it is meant that we have no data available.
Table VII	$\chi_{\|\|}$ v.s. J for $L = 32$ and $L = 48$.

Figure Captions

Fig. 1 Σ v.s. J for $\kappa = 0.47$ and $L = 32$. Circle indicates $\Sigma_{\epsilon,||}$, square is $\Sigma_{\epsilon,\perp}$, and triangle corresponds to $\Sigma_{p,\perp}$. For small J there is a significant difference between the ϵ- and p-expansions. The arrow shows the mean value of $\Sigma_{\epsilon,s}$, as a reference, which is calculated from $\Sigma_{\epsilon,s}$ at seven J points in Table I. The value $\Sigma_{\epsilon,s}$ is regarded as the best estimate of Σ. Detail about $\Sigma_{\epsilon,s}$ is found in the latter part in this section.

Fig. 2 F v.s. J for $\kappa = 0.47$ and $L = 32$. Circle indicates $F_{\epsilon,||}$, square is $F_{\epsilon,\perp}$, and triangle corresponds to $F_{p,\perp}$. The location of the arrow shows the mean value of $F_{\epsilon,s}$, as a reference, which is estimated in the same manner as in Fig. 1 from Table I. It is also the best estimate of F.

Fig. 3 Σ v.s. J for $\kappa = 0.462$ and $L = 32$. Circle indicates $\Sigma_{\epsilon,||}$, square is $\Sigma_{\epsilon,\perp}$, and triangle corresponds to $\Sigma_{p,\perp}$. For $J \gtrsim 2.0 \times 10^{-4}$ the ϵ-expansion appears out of validity. The arrow shows the mean value of $\Sigma_{\epsilon,s}$.

Fig. 4 Σ v.s. J for $L = 32$. All of the values Σ are determined by the scalar product correlation functions. $\Sigma_{\epsilon,s}$ is almost independent of J for both the κ values. For $\kappa = 0.47$ $\Sigma_{p,s}$ (square) agrees with $\Sigma_{\epsilon,s}$ (circle) at $J \gtrsim 3.0 \times 10^{-4}$, while for $\kappa = 0.462$ there is a significant difference between $\Sigma_{\epsilon,s}$ (filled circle) and $\Sigma_{p,s}$ (filled square). The statistical errors of $\Sigma_{\epsilon,s}$ lie within the symbols.

Fig. 5 F v.s. J for $L = 32$. All of the values F are determined by the scalar product correlation functions. Similar behavior to Σ in Fig. 4 is observed. The same symbols as those in Fig. 4 are used.

Fig. 6 Σ determined by the scalar product correlation functions at $L = 48$ and for $\kappa = 0.462$. $\Sigma_{p,s}$ (square) agrees with $\Sigma_{\epsilon,s}$ (circle) at $J = 2.0 \times 10^{-4}$. As seen in Table IV, the p-expansion does not provide reasonable value for $\Sigma_{p,s}$ at $J = 0.5 \times 10^{-4}$, i.e, out of validity. The arrow shows the mean value of $\Sigma_{\epsilon,s}$.

Fig. 7 F v.s. J at $L = 48$ and for $\kappa = 0.462$. $F_{p,s}$ (square) agrees with $F_{\epsilon,s}$ (circle) at $J = 2.0 \times 10^{-4}$. The arrow indicates the mean value of $F_{\epsilon,s}$

Fig. 8 Magnetization $\langle \varphi^0 \rangle$ v.s. J for $L = 32$. Normalization of the data is done at $J = 3.0 \times 10^{-4}$ for $\kappa = 0.47$ and at $J = 2.0 \times 10^{-4}$ for $\kappa = 0.462$. The solid lines show (2.5)(ϵ-expansion), and the dotted lines correspond to (2.19)(p-expansion). A clear crossover between the two expansions is observed for both $\kappa = 0.47$ (square) and $\kappa = 0.462$ (circle).

Fig. 9 Longitudinal susceptibility $\chi_{||}$ v.s. J for $L = 32$. The solid lines show (2.18) (ϵ-expansion), and the dotted lines correspond to (2.28) (p-expansion).

Σ

$J(\times 10^{-4})$	$\epsilon, \|\|$	$\epsilon, \perp$	ϵ, s	$p, \perp$	p, s
0.0	0.2590(8)	0.2569(8)	0.2579(3)	***	***
0.5	0.2577(8)	0.2576(9)	0.2573(4)	###	0.3780(5)
1.0	0.2567(10)	0.2603(17)	0.2577(3)	0.272(2)	0.285(2)
2.0	0.2577(11)	0.259(3)	0.2581(3)	0.256(3)	0.276(4)
3.0	0.2582(11)	0.255(4)	0.2589(4)	0.253(4)	0.261(5)
4.0	0.2560(9)	0.262(5)	0.2585(4)	0.261(5)	0.262(6)
5.0	0.2546(11)	0.262(7)	0.2592(4)	0.261(7)	0.265(8)

F

$J(\times 10^{-4})$	$\epsilon, \|\|$	$\epsilon, \perp$	ϵ, s	$p, \perp$	p, s
0.0	0.290(4)	0.282(3)	0.286(3)	***	***
0.5	0.289(4)	0.286(4)	0.287(4)	###	0.412(5)
1.0	0.279(4)	0.291(5)	0.285(3)	0.231(5)	0.312(5)
2.0	0.280(5)	0.292(6)	0.287(3)	0.274(6)	0.305(5)
3.0	0.272(5)	0.290(6)	0.290(4)	0.284(7)	0.292(6)
4.0	0.257(5)	0.292(7)	0.283(3)	0.290(7)	0.287(7)
5.0	0.245(6)	0.298(10)	0.287(4)	0.297(10)	0.293(9)

$L = 32, \kappa = 0.47$

Table I

Σ

$J(\times 10^{-4})$	$\epsilon, \|\|$	$\epsilon, \perp$	ϵ, s	$p, \perp$	p, s
0.0	0.2050(9)	0.2029(8)	0.2040(5)	***	***
0.5	0.2042(8)	0.2052(10)	0.2040(5)	###	0.3545(6)
1.0	0.2041(9)	0.2046(13)	0.2036(5)	0.213(3)	0.2276(12)
2.0	0.2057(10)	0.2031(19)	0.2047(7)	0.195(2)	0.218(3)
3.0	0.2003(13)	0.214(3)	0.2053(5)	0.210(3)	0.225(4)
4.0	0.1996(16)	0.214(4)	0.2053(6)	0.212(4)	0.220(5)
5.0	0.1975(17)	0.214(4)	0.2062(7)	0.212(4)	0.222(5)

F

$J(\times 10^{-4})$	$\epsilon, \|\|$	$\epsilon, \perp$	ϵ, s	$p, \perp$	p, s
0.0	0.229(4)	0.223(4)	0.226(3)	***	***
0.5	0.232(4)	0.232(5)	0.231(4)	###	0.387(7)
1.0	0.225(5)	0.229(5)	0.227(4)	0.165(4)	0.250(5)
2.0	0.222(5)	0.226(5)	0.225(4)	0.202(5)	0.238(6)
3.0	0.197(5)	0.244(5)	0.224(3)	0.236(5)	0.244(5)
4.0	0.191(6)	0.237(6)	0.220(4)	0.234(6)	0.234(5)
5.0	0.181(5)	0.241(6)	0.223(4)	0.239(6)	0.239(6)

$L = 32, \kappa = 0.462$

Table II

Σ

$J(\times 10^{-4})$	$\epsilon, \|\|$	$\epsilon, \perp$	ϵ, s	$p, \perp$	p, s
0.0	0.2575(9)	0.2576(9)	0.2576(2)	***	***
0.5	0.2585(13)	0.256(4)	0.2578(5)	0.255(4)	0.278(5)
1.0	0.2565(7)	0.264(4)	0.25774(20)	0.263(4)	0.272(6)
3.0	0.2549(7)	0.268(8)	0.2583(3)	0.268(8)	0.270(9)

F

$J(\times 10^{-4})$	$\epsilon, \|\|$	$\epsilon, \perp$	ϵ, s	$p, \perp$	p, s
0.0	0.288(4)	0.286(5)	0.287(4)	***	***
0.5	0.286(6)	0.290(8)	0.290(6)	0.264(8)	0.312(9)
1.0	0.274(4)	0.294(7)	0.284(3)	0.290(7)	0.300(8)
3.0	0.247(5)	0.300(10)	0.285(4)	0.300(10)	0.298(10)

$L = 48, \kappa = 0.47$

Table III

Σ

$J(\times 10^{-4})$	$\epsilon, \|\|$	$\epsilon, \perp$	ϵ, s	$p, \perp$	p, s
0.0	0.2037(5)	0.2023(6)	0.2030(3)	***	***
0.5	0.2023(11)	0.2049(18)	0.2028(6)	0.203(2)	###
2.0	0.2002(15)	0.204(6)	0.2052(5)	0.203(6)	0.206(6)
3.0	0.140(5)	0.846(9)	0.1991(9)	0.204(8)	0.205(9)

F

$J(\times 10^{-4})$	$\epsilon, \|\|$	$\epsilon, \perp$	ϵ, s	$p, \perp$	p, s
0.0	0.229(3)	0.225(4)	0.227(3)	***	***
0.5	0.220(6)	0.228(7)	0.224(5)	0.197(6)	###
2.0	0.188(7)	0.236(8)	0.230(5)	0.235(8)	0.231(7)
3.0	0.113(9)	1.13(3)	0.205(6)	0.229(11)	0.225(11)

$L = 48, \kappa = 0.462$

`Table IV`

Σ

κ	$\epsilon, \|\|$	$\epsilon, \perp$	ϵ, s
0.460	0.1841(12)	0.1831(12)	0.1836(7)
0.462	0.2025(6)	0.2031(6)	0.2028(3)
0.470	0.2580(8)	0.2569(10)	0.2574(2)

F

κ	$\epsilon, \|\|$	$\epsilon, \perp$	ϵ, s
0.460	0.206(6)	0.205(7)	0.206(7)
0.462	0.225(4)	0.223(4)	0.224(4)
0.470	0.288(5)	0.284(5)	0.286(4)

$L = 64, J = 0.0$

`Table V`

$J(\times 10^{-4})$	$\langle\varphi^0\rangle$ at $\kappa = 0.462$	$\langle\varphi^0\rangle$ at $\kappa = 0.47$
0.0	−0.0009(17)	−0.0016(14)
0.5	0.0811(15)	0.1209(17)
1.0	0.1486(14)	0.208(2)
2.0	0.2339(13)	0.3047(15)
3.0	0.2662(11)	0.3405(12)
4.0	0.2851(8)	0.3557(9)
5.0	0.2951(9)	0.3644(9)

$L = 32, \langle\varphi^0\rangle$

$J(\times 10^{-4})$	$\langle\varphi^0\rangle$ at $\kappa = 0.462$	$\langle\varphi^0\rangle$ at $\kappa = 0.47$
0.0	0.0002(13)	0.0018(18)
0.5	0.201(2)	0.279(2)
1.0	%%%	0.3372(13)
2.0	0.2940(7)	%%%
3.0	0.3045(8)	0.3726(7)

$L = 48, \langle\varphi^0\rangle$

Table VI

$J(\times 10^{-4})$	$\chi_{\vert\vert}$ at $\kappa = 0.462$	$\chi_{\vert\vert}$ at $\kappa = 0.47$
0.0	1710.10(5)	2545.59(7)
0.5	1534.67(12)	2166.94(17)
1.0	1183.82(15)	1508.6(3)
2.0	523.61(18)	522.3(3)
3.0	250.24(17)	213.9(2)
4.0	136.08(12)	106.70(18)
5.0	97.89(15)	77.62(17)

$L = 32, \chi_{||}$

$J(\times 10^{-4})$	$\chi_{\vert\vert}$ at $\kappa = 0.462$	$\chi_{\vert\vert}$ at $\kappa = 0.47$
0.0	5438.72(6)	8258.40(15)
0.5	2311.5(5)	2447.5(7)
1.0	%%%	589.7(4)
2.0	148.9(2)	%%%
3.0	71.5(2)	72.9(3)

$L = 48, \chi_{||}$

Table VII

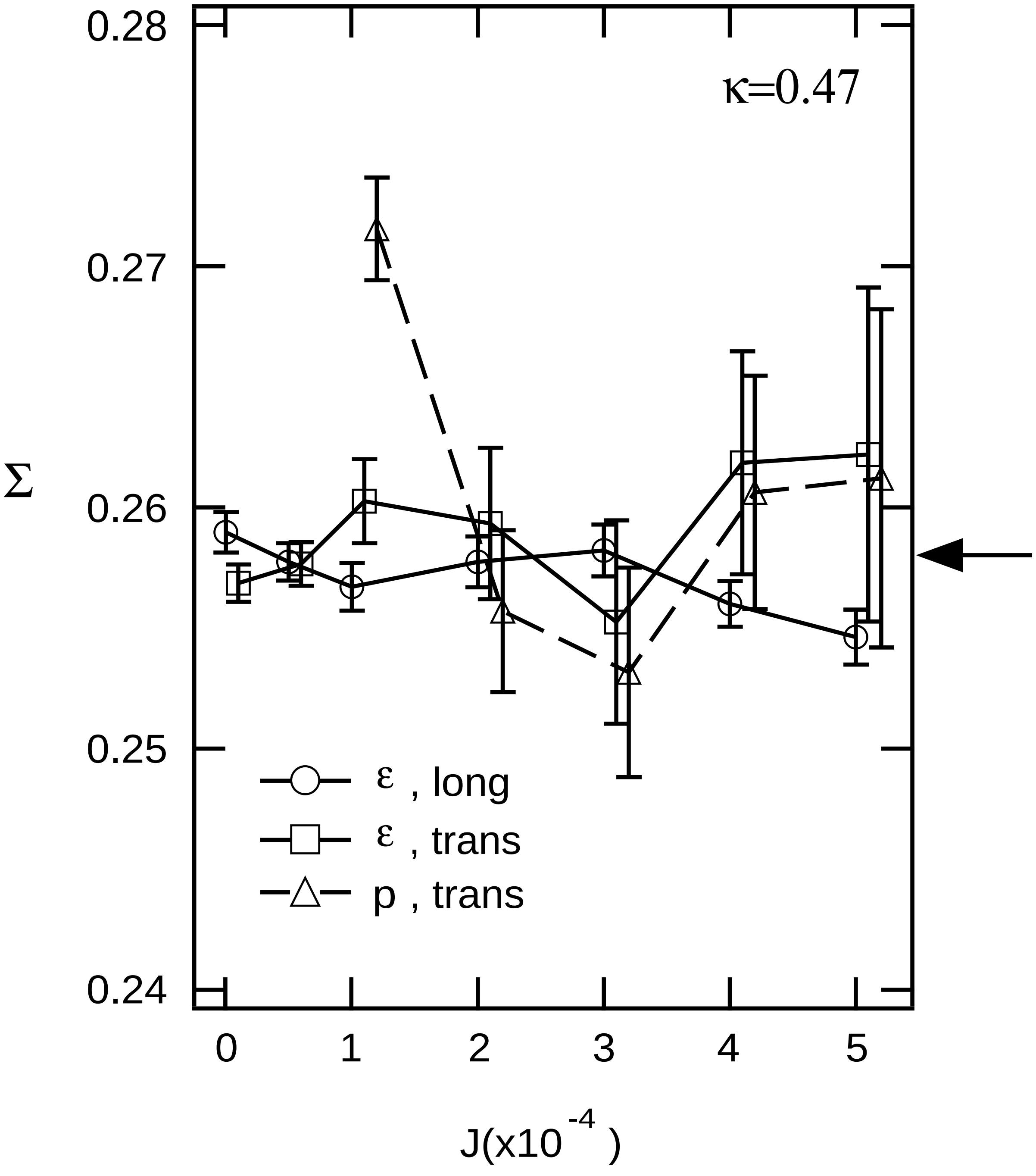

Fig.1

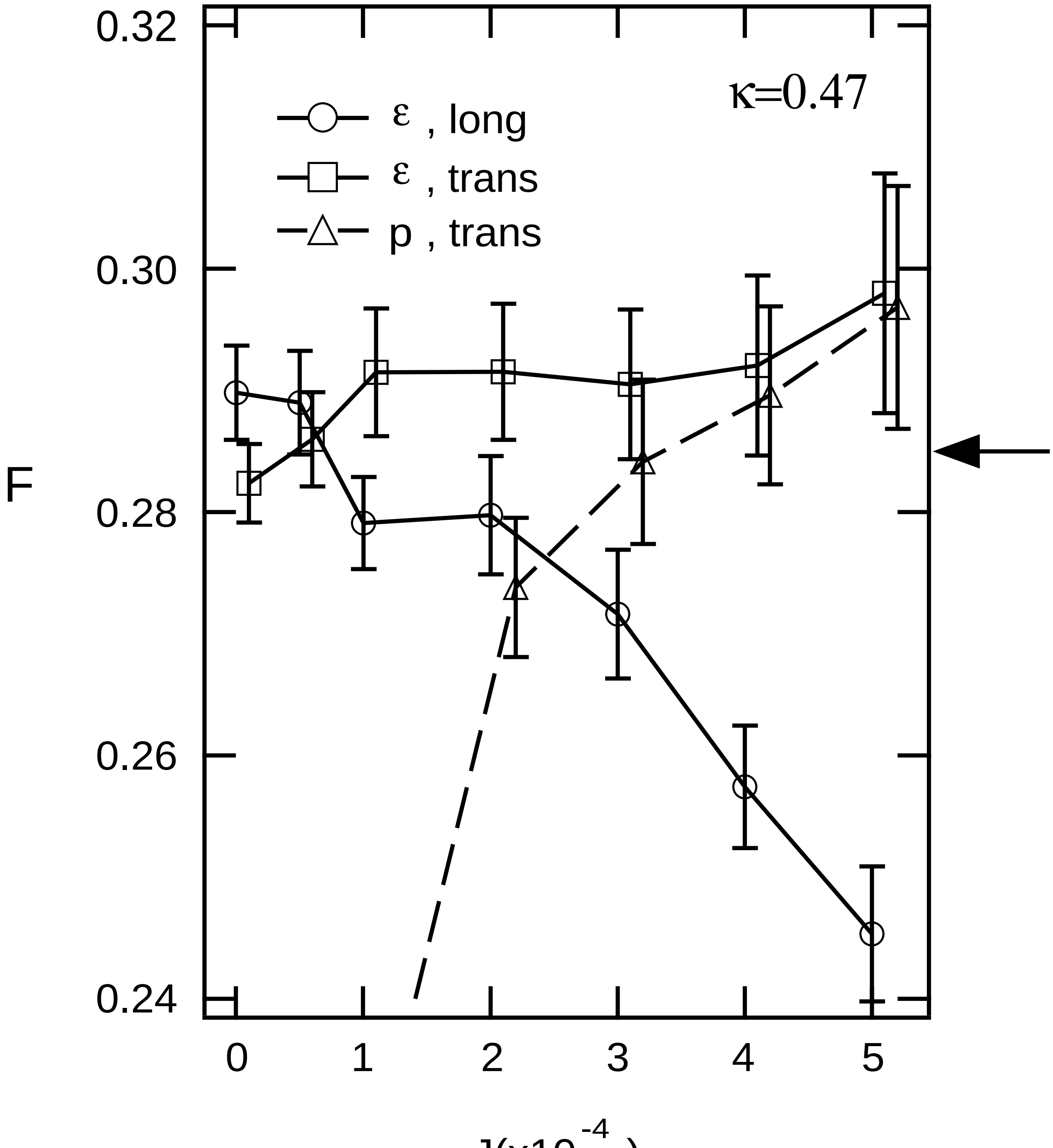

Fig.2

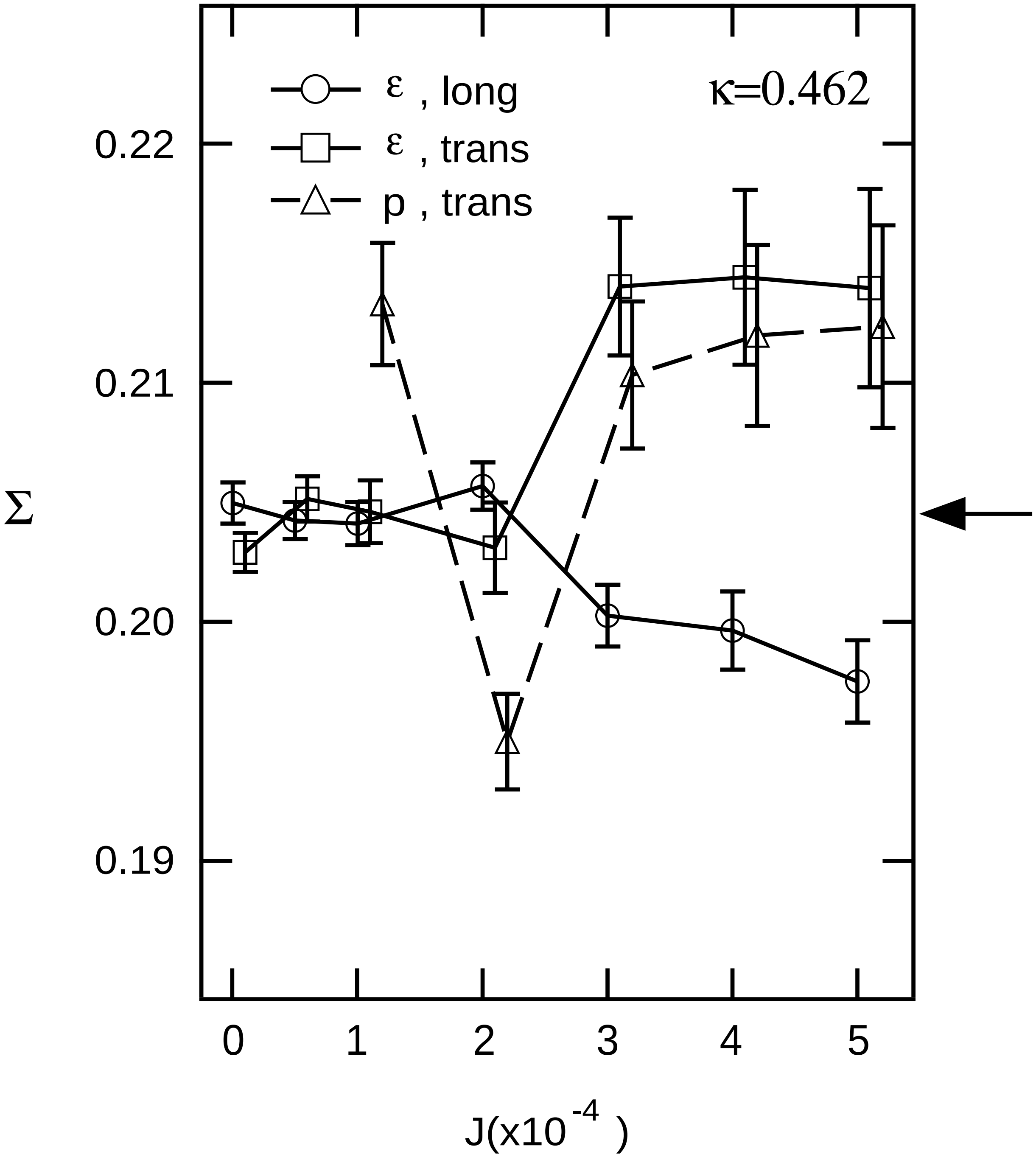

Fig.3

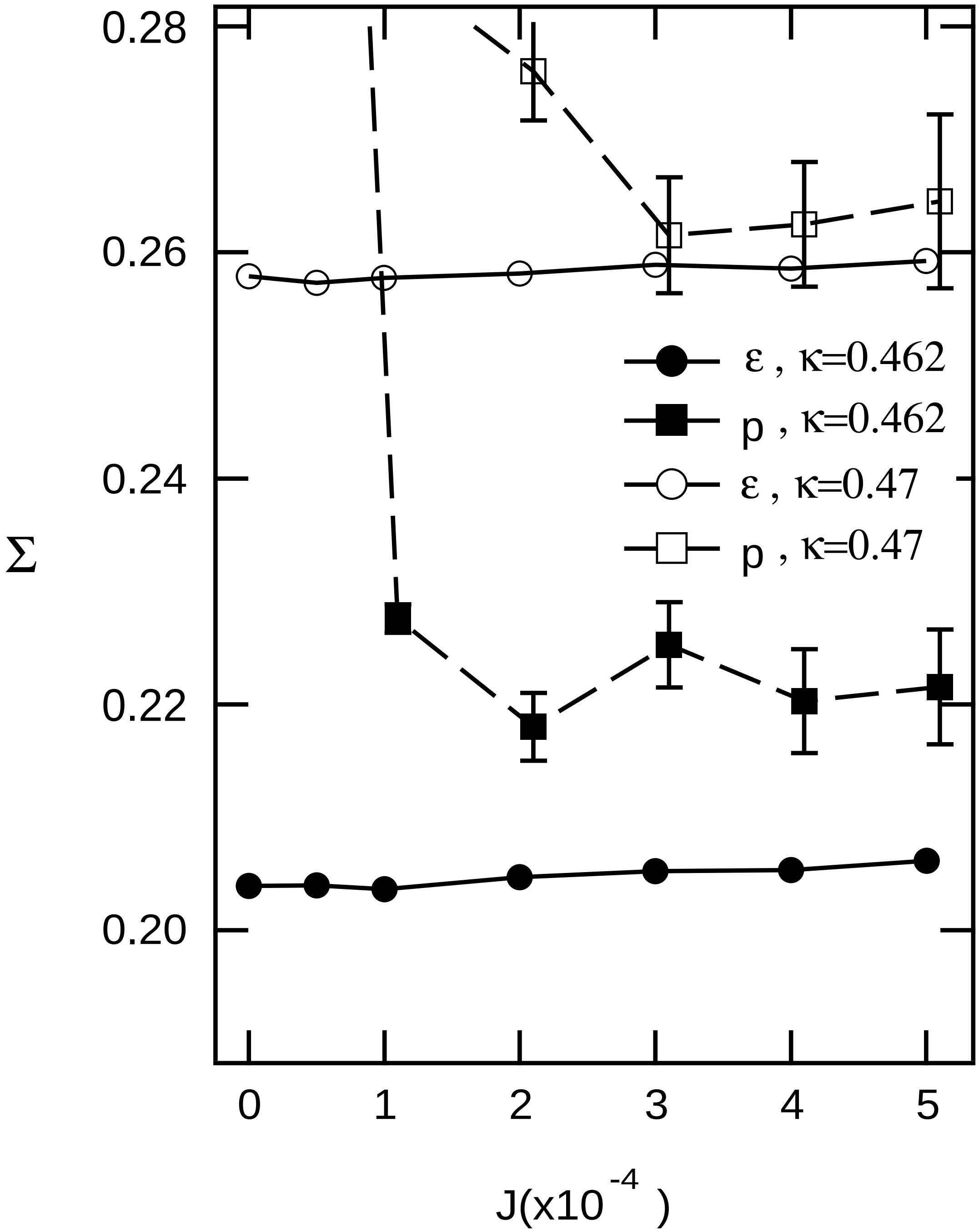

Fig.4

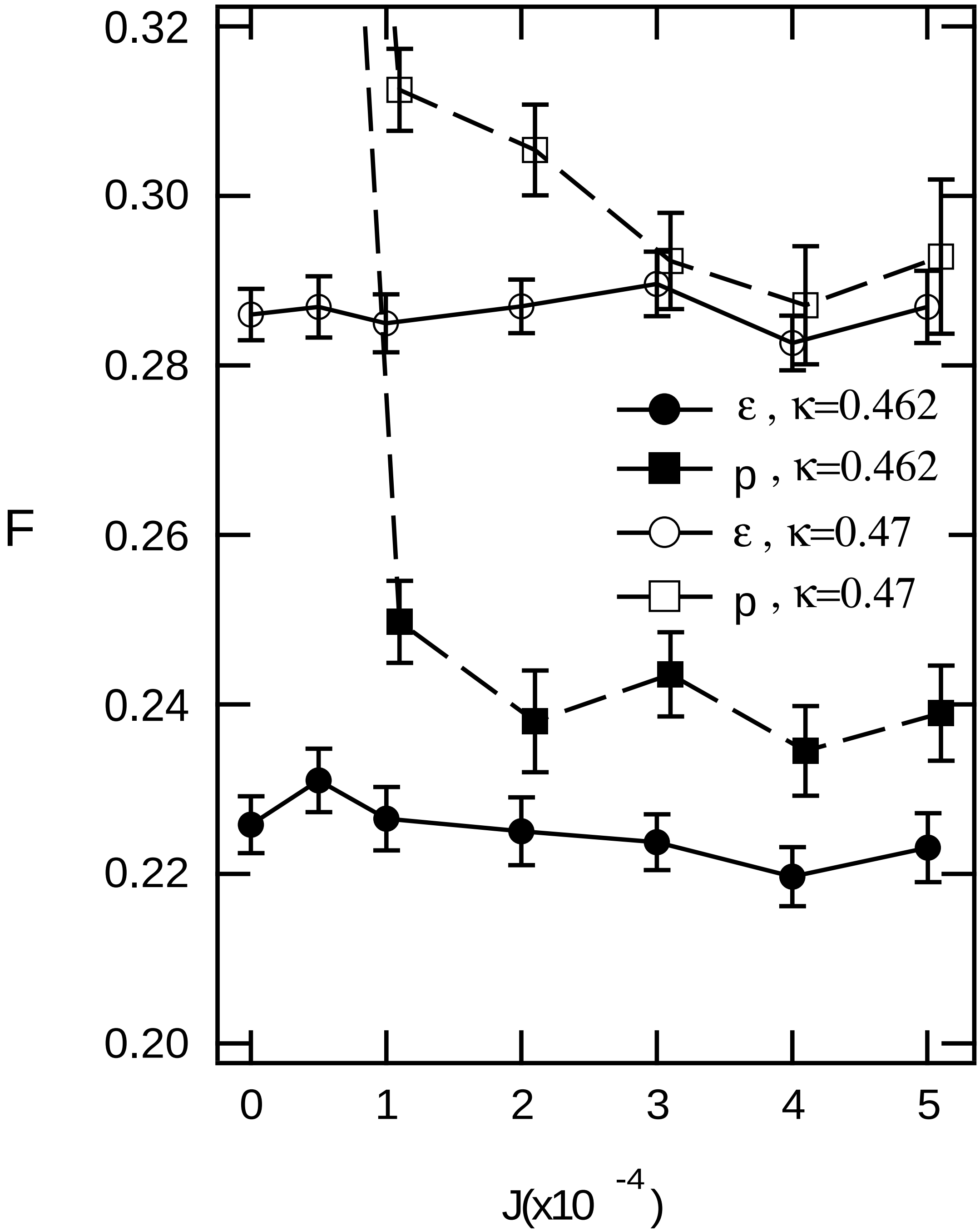

0.32
0.30
0.28
0.26
0.24
0.22
0.20
F
0
1
2
3
4
5
J(x10 -4)
ε , κ=0.462
p , κ=0.462
ε , κ=0.47
p , κ=0.47

Fig.5

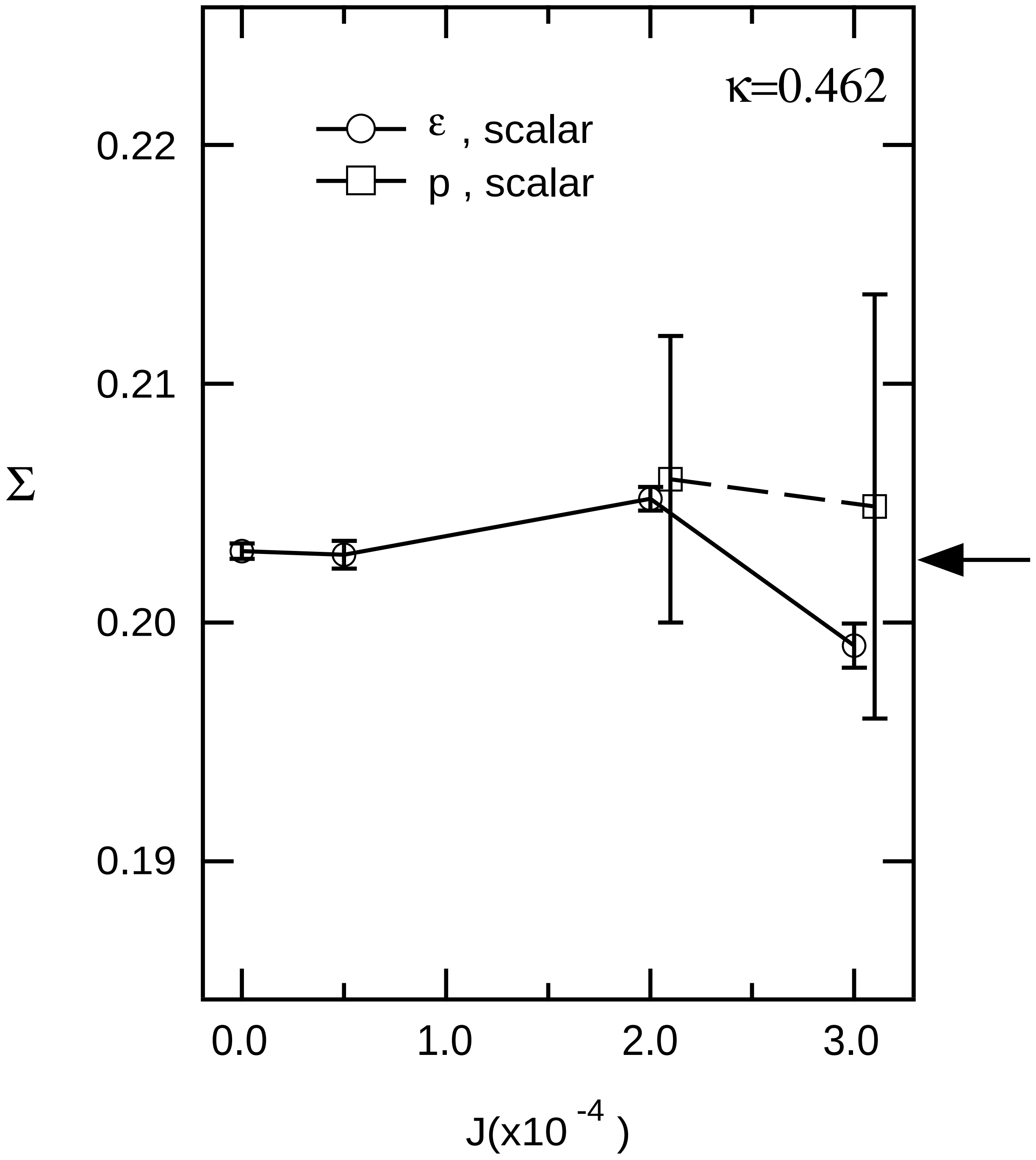

Fig.6

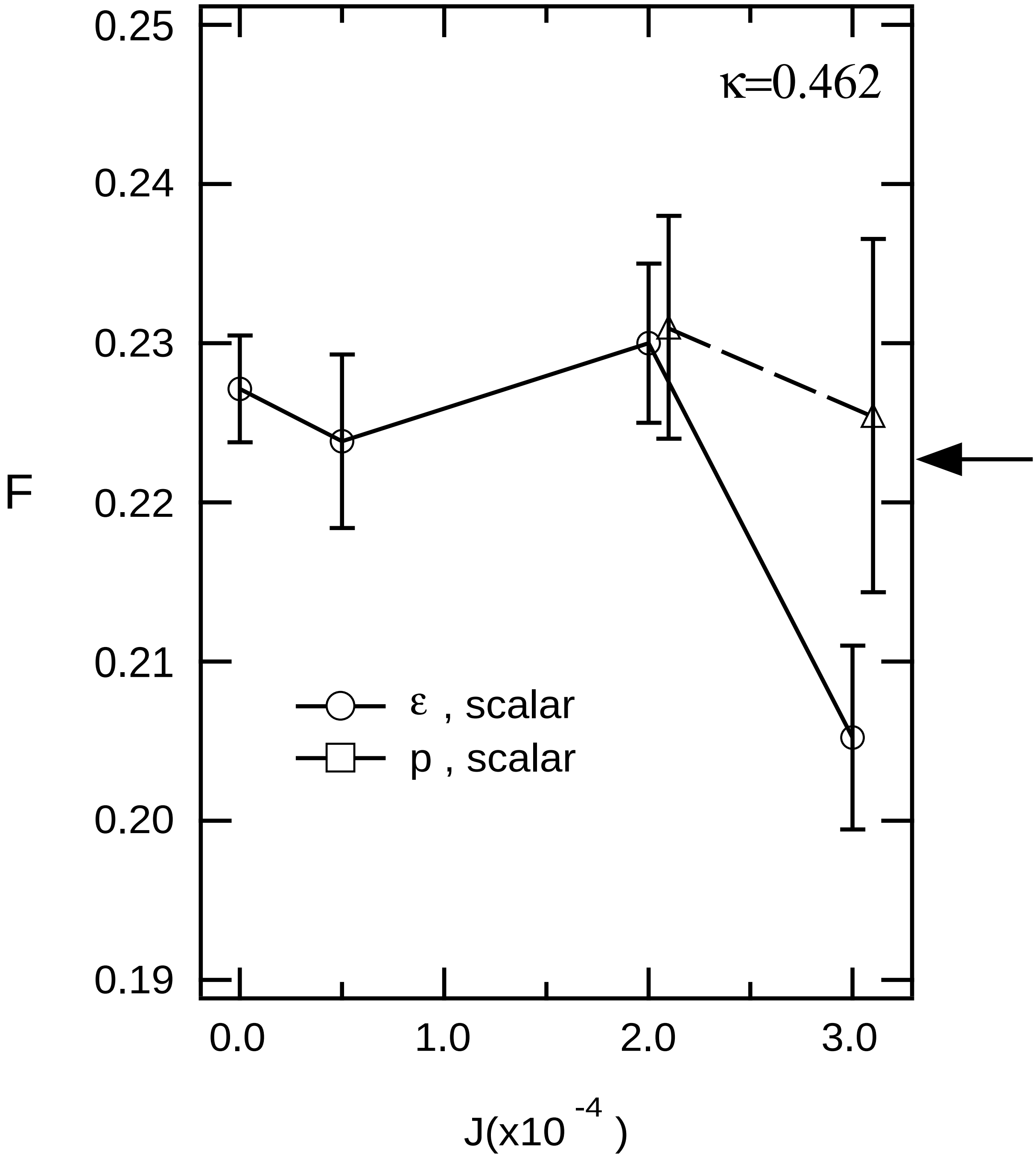
κ=0.462
F
0.25
0.24
0.23
0.22
0.21
0.20
0.19
0.0
1.0
2.0
3.0
J(x10 -4)
ε , scalar
p , scalar

Fig.7

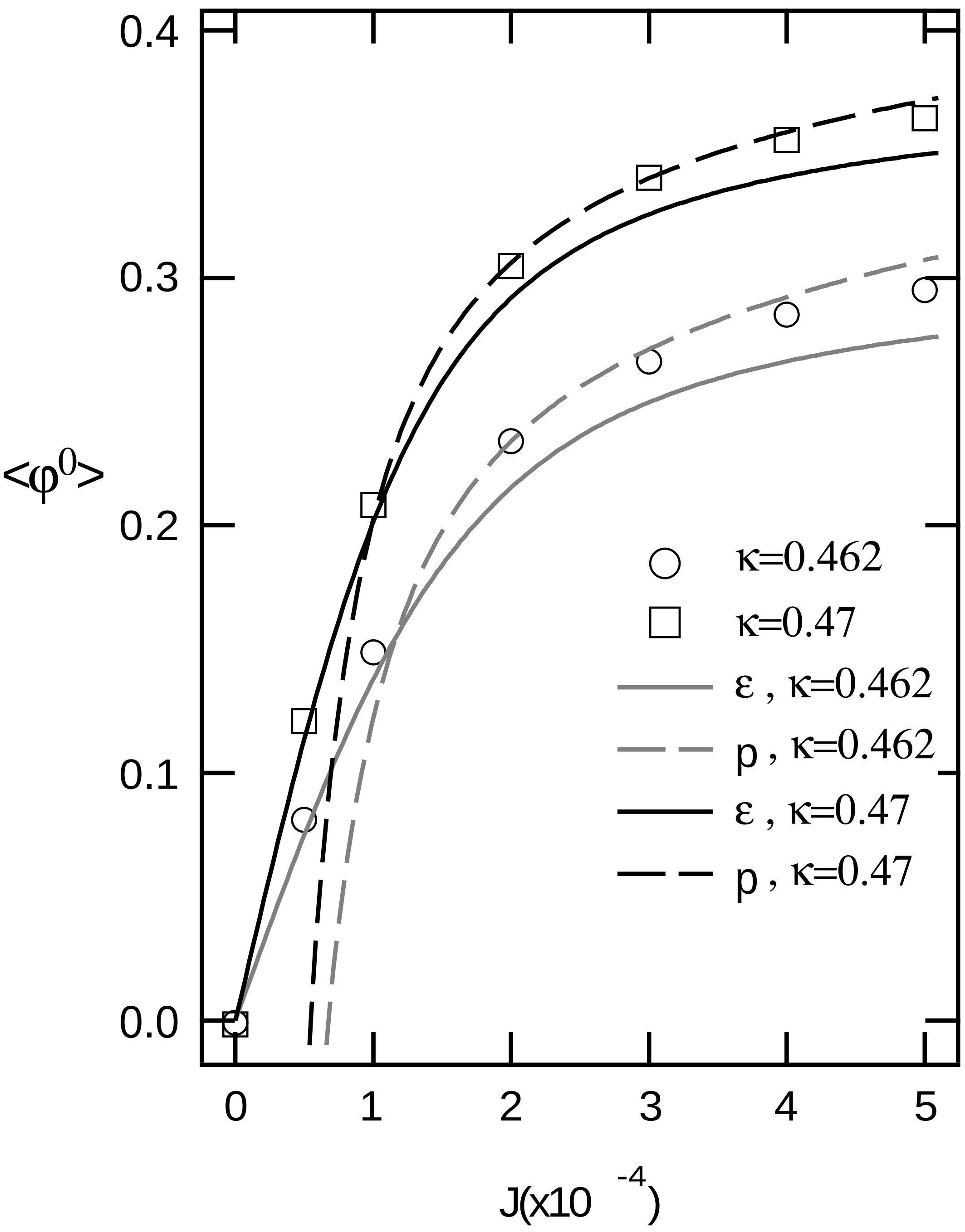

0.4
0.3
0.2
0.1
0.0
<φ0>
0
1
2
3
4
5
J(x10 -4)
κ=0.462
κ=0.47
ε , κ=0.462
p , κ=0.462
ε , κ=0.47
p , κ=0.47

Fig.8

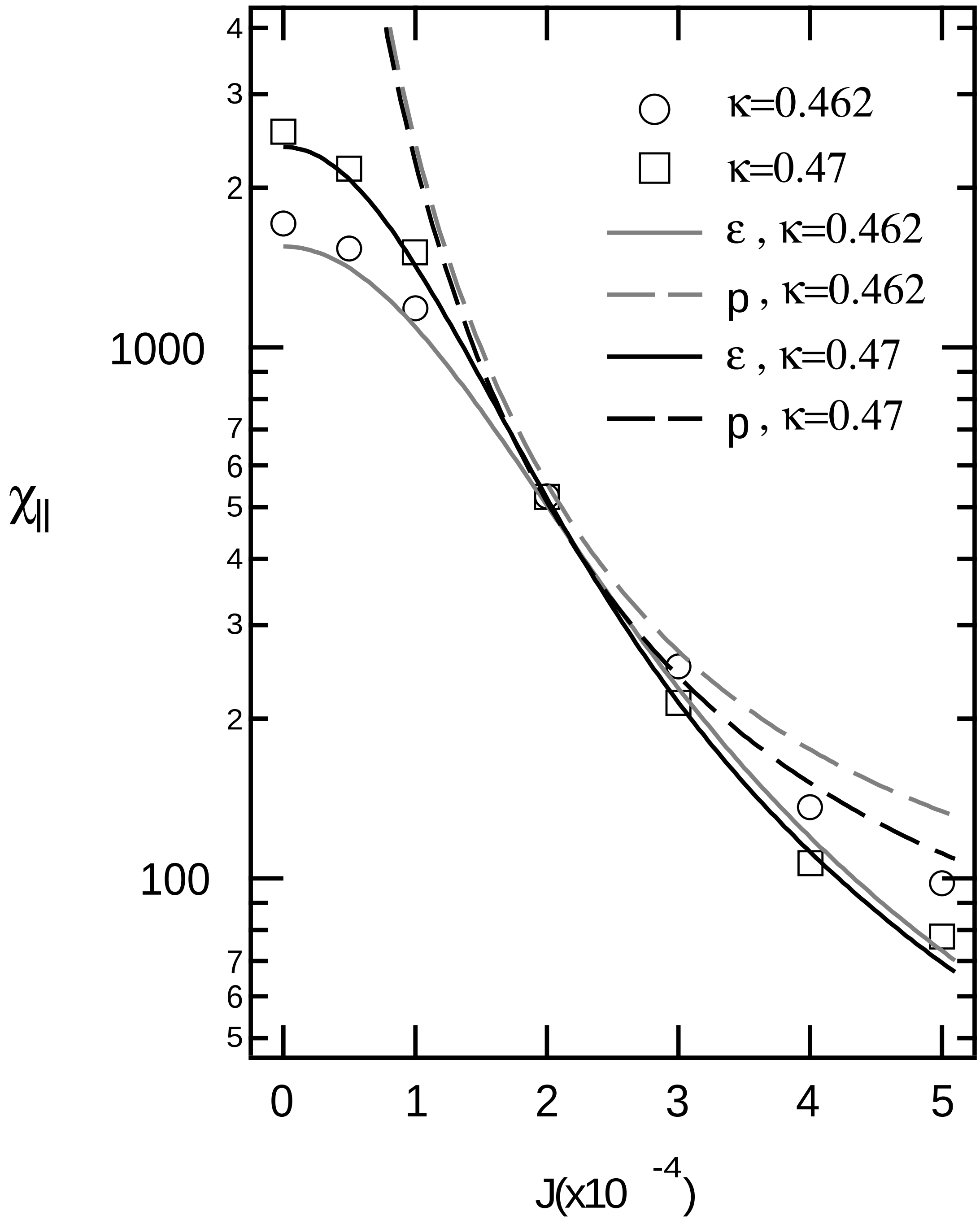

χ∥
J(x10 -4)
0
1
2
3
4
5
100
1000
5
6
7
2
3
4
κ=0.462
κ=0.47
ε , κ=0.462
p , κ=0.462
ε , κ=0.47
p , κ=0.47

Fig.9